CAPILLARY SUCTION MODEL AS PIPES OF DIFFERENT SIZES: FLOW CONDITIONS AND COMPARISON WITH EXPERIMENTS

Hung Thanh Nguyen[1] Stefan Jacobsen[2] , Frank Melandsø[3]

[1]Narvik University College, Norway
[2]Norwegian University of Science and Technology, Trondheim, Norway
[3]University of Tromsø, Norway

ABSTRACT

Absorption of water in concrete is often described by the simple linear water uptake vs. square-root-of-time law. However, a deviation from this behaviour is frequently seen depending on factors such as initial water content, water/binder ratio and specimen thickness. The deviation increases with thickness (typically from 25 to 100 mm) and is seen even for very dry specimens with capillary pores. We have applied Laplaces law for suction created under a curved meniscus between air and water to series of pipes with different lengths and radii. The resulting analytical model was first compared with numerical simulations at abrupt reduction or increase of pipe radius showing good agreement. Then a complete second order equation describing the relation between the capillary suction and the suction time was developed. Varying geometries of the pipes of the capillary system were investigated including the effects on the flow rate of varying combination of lengths, radii and sequence. The results showed that largest flow reductions occurred with very narrow sections causing a blocking, reducing the capillary flow rate vs. square root of time in the same manner as in concrete. The often observed phenomenon of reduced flow below the straight line water uptake vs. square root of time could be simulated with the multiple diameter pipe models, as seen by comparing simulations with experiments with varying concrete qualities and sample thicknesses in simple capillary absorption tests.

Key-words: capillary suction, pipe geometry, model

INTRODUCTION

Capillary transport of water in concrete has kept the attention of researchers world wide for many years. It is considered a basic transport mechanism [1] and mainly ascribed to suction under water meniscii in capillary pores. During the last decade an increasing portion of the applied concrete qualities has very low capillary porosity due to increasing use of low

water/binder ratios and supplementary cementing materials like fly ash and condensed silica fume that refine and make the pore structure less continuous [2]. However, such concretes may, after some predrying of thin specimens, still show the typical nick point on the water uptake vs square root of time plots from one sided (unidirectional) capillary suction experiments. The characteristic nick point absorption is associated with the existence of capillary porosity. The severity of drying has a very clear effect, and this has been found to relate to the degree of saturation of the pore system at start [3]. By re-plotting these results they actually fit well into the kind of saturation-sorptivity plots suggested [1] for use in solving Richards equation. However, in experiments there is a size effect on capillarity that is problematic compared to the capillary mechanism since there is an increasing deviation from the linear absorption vs square root of time relation of capillary theory as the sample thickness is increasing. The size dependant deviation from the square root-law effect has sometimes been ascribed to the replacement of interstitial water and subsequent swelling of the gel [1]. We, however, believe that capillary discontinuities in the form of narrow passages or larger capillary voids along the flow path of the capillary pore system can be involved in the phenomenon (as some sort of pipe geometry effect on the water transport). Depending on the severity of pre-drying the deviation from the square-root law has been observed in concrete with a significant amount of capillary porosity [4] as well as in HPC materials with little capillary porosity [3]. The deviation has also been observed in capillary absorption experiments with an organic fluid [5]. It is therefore probable that the proposed gel swelling [1] cannot be a general explanation for the anomaly. Figure 1 shows the results of one of our experiments on cylindrical mortar specimens with diameter 100 mm and w/c = 0.60 after drying at 105 C.

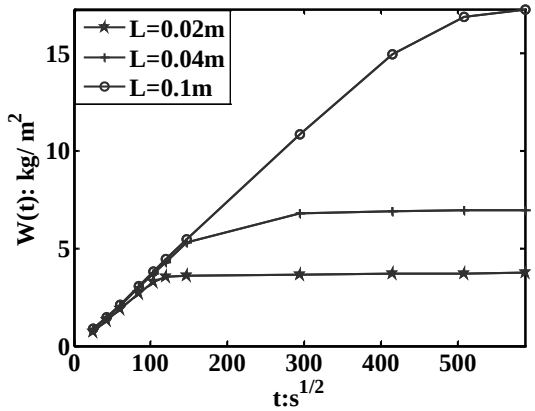

Figure 1- Capillary absorption in w/c 0.60 mortar with increasing deviation from linear absorption vs square-root-of-time law at increasing specimen thickness 20 to 40 to 100 mm.

Figure 1 shows how real capillary absorption deviates increasingly from the square-root of time law as the specimen thickness increases from 20 to 40 to 100 mm height. We also see how the nick-points become less distinct at increasing specimen height. In this paper we investigate the above phenomenon with a combined experiment-modelling approach with different pipes representing the capillary pore system [6,7].

CAPILLARY SUCTION FLOW MODELS

Varying pipe flow approaches have been taken in earlier studies of this kind of problem. Some have been based on pipe flow according to Hagen-Poiselle (HP) with capillary suction due to the under-pressure caused by the surface tension between liquid and gas $\sigma_{l\text{-}g}$ (l-g -

water-air in our case) and the curvature of the water meniscus between air and the liquid wetting the pipe wall (concrete in our case). One example of pipe flow modelling can be found in [8] and early efforts to model capillary suction in sandstone and concrete in this way are [9,10]. However, these studies did not analyse the reasons for the increasing deviation from the square root of time law as the specimen thickness increases.

Flow modelling by suction in pipes with stepwise changing radius

As a starting point for our capillary system, we will assume an incompressible and stationary flow in an axial-symmetric pipe system driven by the suction under the water meniscus between water and air. Outside the pipes there is no porosity. Thus, on a multiscale we neither consider the transport mechanisms in nanoscopic gel pores nor macroscopic air voids; only the microscopic capillaries. In order to develop an analytical capillary model for a pipe system with a stepwise changing cross section, we will start with the two-sized model shown in Figure 2. This Figure illustrates how a physical flow pattern shown in the upper Figure 2(a), can be approximated with the stepwise model shown in the upper Figure 2(b). For this binary model we assume a HP flow in both sections, which changes abruptly at the interface ($x = x_1$). Thus we neglect the regions indicated with the darkest shading in the upper Figures, where the flows are not fully developed. This approach will also lead to a stepwise flow velocity and a linear pressure as indicated in the lower Figure 2(b), acting as approximation for the physical mean fields shown in the lower Figure 2(a).

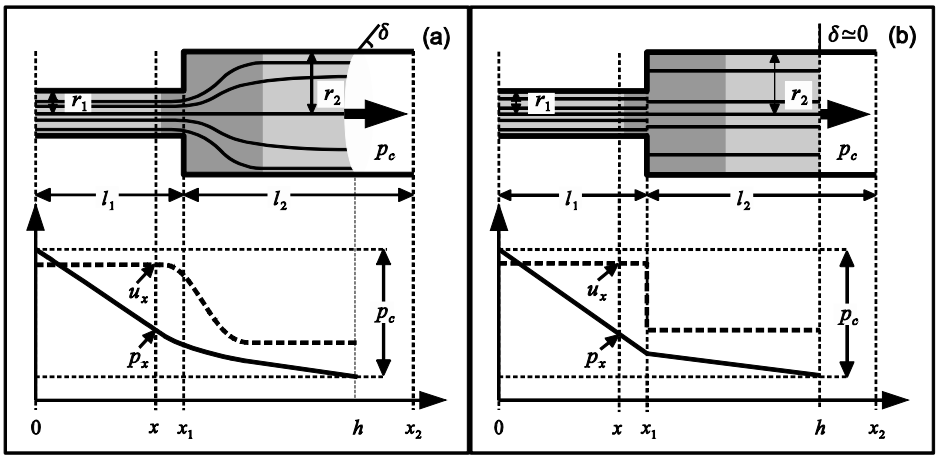

Figure 2- A circular tube divided into two sections and the balance force between the capillary force p_c under the water meniscus and the moving-body-force.

The velocity field u_x and pressure field p_x should be considered as mean values over the pipe cross section. These are deduced from mass- and momentum conservation [6] for an axial-symmetrical flow:

$$u_x = \frac{2}{r_x^2}\int_0^{r_x} u(r,x)\ r\ dr \quad \text{and} \quad p_x = \frac{2}{r_x^2}\int_0^{r_x} p(x,r)\ r\ dr \tag{1}$$

In addition to the radius parameter r_x which has the value r_1 and r_2 in section 1 and 2, respectively, the geometry is also characterized by the sections length l_1 and l_2, and h which is the current position for the water front. Local expressions for the HP flow for fully developed flow profiles are obtained from integration with non-slip boundary conditions as reviewed in [6] yielding the well known parabolic HP-profile [11] in each pipe section:

$$u(x,r) = -\frac{1}{4\mu}\left(\frac{dp_x}{dx}\right) r_x^2 \left[1 - \left(\frac{r}{r_x}\right)^2\right] \tag{2}$$

Where μ is viscosity [Pa·s]. This result may be used to determine the mean velocity of flow. After substituting eq. (2) into the first of eqs. (1) and integrating, we obtain:

$$u_x = -\left(\frac{r_x^2}{8\mu}\right)\left(\frac{dp_x}{dx}\right). \tag{3}$$

It should be emphasized that both the pipe radius, the pressure gradient and the velocity in eq. (3) are local quantities changing between the individual pipe sections. Therefore, in order to determine the velocity at the fluid-front u_h based on eq. (3), we need two additional conditions. The first condition is the pressure fall from position $x = 0$ to h. This pressure fall has to be balanced by the capillary suction under- pressure p_c at the water front as shown in Figure 2. The second condition is the conservation of water flow, i.e. the volume flowing through a cross section at the left side per time unit must be equal to the volume flowing through a section at the right hand side.

Capillary suction under curved mensiscus in pipe series – analytical model

The first condition, the capillary suction (or under-pressure p_c in Figure 2), can at moderate velocities be approximated with the stationary pressure given by the Laplace equation (eq.(4))

$$p_c = -\frac{2\sigma_{l-g}\cos\delta}{r_h} \tag{4}$$

obtained from static conditions. Here σ_{l-g} is the surface tension between water and air and δ the contact angle between the pipe wall and the wetting water front (see for example [1],[12]). The second condition gives [13]:

$$u_x A_x = u_h A_h \Rightarrow u_x = u_h \frac{r_h^2}{r_x^2}. \tag{5}$$

Here A_x and A_h are the cross section areas at position x and h, respectively, as shown in Fig. 2(b). After rearranging eq. (3) and then integrating from $x = 0$ to h we obtain

$$\int_0^h u_x \frac{dx}{r_x^2} = \frac{1}{8\mu}\left(-\int_{p_0}^{p_h} dp_x\right) \tag{6}$$

A further reformulation of this equation can be done by inserting expressions for the pressure $p_c = p_h - p_0$ and velocity u_x given by eqs. (4) and (5), respectively. This yields

$$u_h = \frac{k}{f(h) r_h^3} \tag{7}$$

for the capillary front velocity where we have introduced a constant k as

$$k = \frac{\sigma_{l-g}\cos\delta}{4\mu}. \tag{8}$$

and a function f depending on the number and size of pipes and the position of the water front

$$f(h) = \int_0^h \frac{dx}{r_x^4} = \frac{l_1}{r_1^4} + \cdots + \frac{l_{j-1}}{r_{j-1}^4} + \frac{h - x_{j-1}}{r_j^4} = \sum_{i=1}^{j-1} f_i + \Delta f_j, \quad \text{with} \quad f_i = \frac{l_i}{r_i^4} \text{ and } \Delta f_j = \frac{(h - x_{j-1})}{r_j^4}. \tag{9}$$

in a model extended from Figure 2 into j pipe sections as shown in Figure 3:

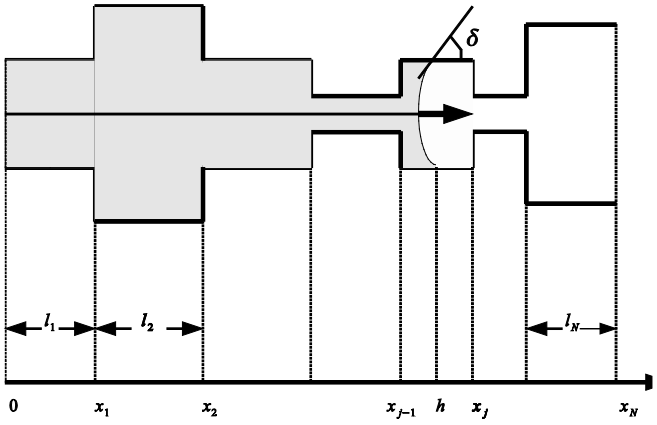

Figure 3- Pipe with $N-$ irregular subsections and water front at the jth section

Then, in order to obtain an equation for the flow u_h at a length (or height) h going through N subsequent pipe sections of different lengths and radii, a general expression was developed extending from the above approach:

$$u_h = \frac{k}{\beta_1/\alpha_1 + \beta_2/\alpha_2 + \ldots + \beta_{j-1}/\alpha_{j-1} + \beta_j/\Delta\alpha_j}. \tag{10}$$

where α describes how rapidly the cross sections change with respect to pipe section length and in relation to position of the water front:

$$\alpha_i = \frac{r_i}{l_i} \quad for \quad i = 1,2,\cdots, j-1, \quad and \quad \Delta\alpha_j = \frac{r_j}{h - x_{j-1}} \tag{11}$$

and β relates the cross sections of previous pipe sections ($i = 1,2,\ldots, j-1$) to the current section ($i = j$) with $\beta_j = 1$ due to its definition:

$$\beta_i = \left(\frac{r_j}{r_i}\right)^3 \quad for \quad i = 1,2,\cdots, j. \tag{12}$$

The relation between the capillary velocity and the capillary height in eq (10) above is also given by the differential equation, eq. (13):

$$u_h = \frac{dh}{dt} \tag{13}$$

which can be inserted in eq. (7) and then integrated. This yields

$$\int_0^h r_s^3 f(s) ds = kt. \tag{14}$$

where s is an integration variable running over the tube sections with a stepwise changing radius r_s and k is, as usual, given by eq. (8). A solution of eq. (14) will for a general variation in the cross section, require a numerical approach [14]. However, for a stepwise changing

radius, it is possible to work out solutions by analytical means. We notice that the function $f(s)$ has to be continuous since it occurred from integrating a stepwise changing function (given by eq. (9)), and linear in the individual tube sections as illustrated in Figure 4.

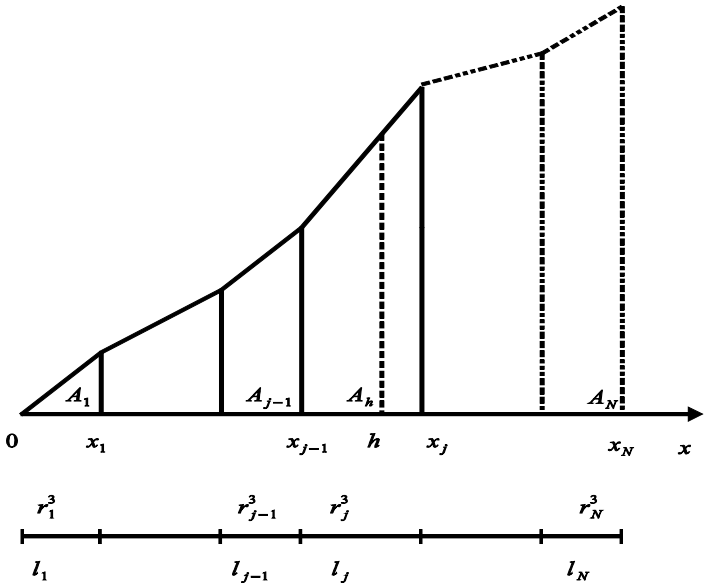

Figure 4- The area under the graph of $f(h)$ *from 0 to* h, $A_1, \cdots, A_h$

The left hand side of eq. (14) may therefore be interpreted as the area A under the graph $f(h)$ from 0 to h weighted by the section value r_h^3, Figure 4. With this in mind and using the analytical formula for $f(h)$ (eq.(9)) and for the area formula of a trapezoidal element, we get:

$$\begin{aligned}\int_0^h r_s^3 f(s)ds &= [r_1^3 A_1]+[r_2^3 A_2]+\cdots+[r_{j-1}^3 A_{j-1}]+[r_j^3 A_h] \\ &= r_1^3\left[\frac{1}{2} f_1 l_1\right]+r_2^3\left[f_1 l_2+\frac{1}{2} f_2 l_2\right]+\cdots \\ &+ r_{j-1}^3\left[(f_1+f_2+\cdots+f_{j-2})l_{j-1}+\frac{1}{2} f_{j-1} l_{j-1}\right] \\ &+ r_j^3\left[(f_1+f_2+\cdots+f_{j-1})+\frac{1}{2}\Delta f_j\right](h-x_{j-1}) \\ &= \left[\sum_{i=1}^{j-1} r_i^3 l_i\left(\sum_{m=1}^{i-1} f_m+\frac{1}{2} f_i\right)\right]+ \\ &\left[r_j^3(h-x_{j-1})\left(\sum_{i=1}^{j-1} f_i+\frac{1}{2}\Delta f_j\right)\right].\end{aligned} \tag{15}$$

From eq. (15) we see that only the terms related to the front section or j-section, is a function of the capillary height h, while the other terms may be regarded as constants with respect to this parameter. Moreover, by inserting eq. (15) into the left side of eq. (14) and by substituting Δf_j from the last to parts of eq. (9), we find that h and time t are related through the following second order equation:

$$\left[\sum_{i=1}^{j-1} r_i^3 l_i \left(\sum_{m=1}^{i-1} f_m + \frac{1}{2} f_i\right)\right] + \left(r_j^3 \sum_{i=1}^{j-1} f_i\right)\Delta h_j + \frac{1}{2r_j}(\Delta h_j)^2 = kt\,. \tag{16}$$

As a short notation we have here introduced the relative height

$$\Delta h_j = h - x_{j-1}, \tag{17}$$

measured from the starting position x_{j-1} from the last section. In addition, we will also introduce the following parameters:

$$C_{j-1} = \sum_{i=1}^{j-1} r_i^3 l_i \left(\sum_{m=1}^{i-1} f_m + \tfrac{1}{2} f_i\right), \qquad B_j = r_j^3 \sum_{i=1}^{j-1} f_i, \qquad \bar{A}_j = \frac{1}{2r_j} \tag{18}$$

to put Eq. (16) into the quadratic form

$$C_j + B_j \Delta h_j + \bar{A}_j \Delta h_j^2 = kt \tag{19}$$

Several useful results may be deduced from eq.(19), for example the required filling time t

$$t = \frac{C_{j-1}}{k} + \frac{B_j \Delta h_j + \bar{A}_j \Delta h_j^2}{k} \tag{20}$$

for all pipe section up to h, for cases where h is specified. Here the first term provides the filling time for the first $(j-1)$ sections while the second term gives the time needed to fill up the last section up to position h. On the other hand, if the total filling time t is known or specified, Δh_j may be obtained from using the quadratic solution formula on eq. (19), to give

$$\Delta h_j(t) = \frac{-B_j + \sqrt{B_j^2 - 4\bar{A}_j(C_{j-1} - kt)}}{2\bar{A}_j} \tag{21}$$

Only the positive root of eq. (21) should be considered here. It is also possible to recalculate well known capillary formulas for tubes with a uniform radius r_U from eq. (19). From $r_1 = r_2 = \cdots = r_j = r_U$ we find:

$$h(t) = \sqrt{2 r_U kt} = \left[\sqrt{\frac{r_U \sigma \cos\delta}{2\mu}}\right]\sqrt{t} \tag{22}$$

often refereed to as the Lucas-Washburn equation [15,16]. Finally, we will show that the previously derived fluid velocity can be expressed in terms of the new notation, e.g. the $\bar{A}-$, $B-$ and $C-$terms introduced in eq. (18). This will give us an analytical expression for the velocity as a function of time. This time relation may be found by derivation of the flow height in eq. (21) with respect to time, which yields eq. (23):

$$u_{\Delta h_j}(t) = \frac{d(\Delta h_j)}{dt} = \frac{d}{dt}\left[\frac{-B_j + \sqrt{B_j^2 - 4\bar{A}_j(C_{j-1} - kt)}}{2\bar{A}_j}\right] = \frac{k}{\sqrt{B_j^2 - 4\bar{A}_j(C_{j-1} - kt)}} \tag{23}$$

One should notice that this equation has to be identical to previous velocity expressions given as a function of position u_h, for example, eq. (7). To show this, the time t in eq. (23) may be replaced by eq. (20). This gives

$$u_h = \frac{k}{\sqrt{B_j^2 - 4\bar{A}_j\left(C_{j-1} - \left(C_{j-1} + B_j\Delta h_j + \bar{A}_j \Delta h_j^2\right)\right)}} = \frac{k}{B_j + 2\bar{A}_j \Delta h_j} = \frac{k}{f(h) r_h^3} \tag{24}$$

Numerical verification of analytical flow model

In order to analyse the flow conditions at the abrupt change in diameter of the analytical model as shown in Figure 2 numerical simulations of the flow conditions at intersections between different small and large pipes were performed. The FEM based numerical tool COMSOL Multiphysics [17] was used for this purpose by solving the flow fields using Navier Stokes equation. Two different geometries were applied; C (Contraction – large pipe leading into small) with $\beta_1 = 0.125$ and model E (Expansion – small pipe leading into large) with $\beta_1 = 8$, see figure 5. In both cases α_2 varied in the order 0.0001 – 1 and $\alpha_1 = \alpha_2/2$ according to the chosen geometry.

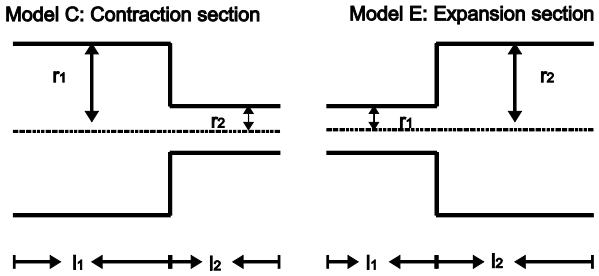

Figure 5- Tube with contraction ($\beta_1 = 0.125$) and expansion ($\beta_1 = 8$) sections

Thus a range of different ratios between length and radii were applied in numerical simulations. The objective was to find out when the analytical models "breaks down" in terms of deviating from the numerical solutions of the not fully developed laminar flow shown at the darkest shading in Figure2 and also analyzed in terms of Reynolds numbers [6]. Figure 6 shows examples of the numerical simulations for the E-model. The absolute value of the pipe flow rate varied considerably; from a bit less than 1 mm/s to a bit more than 1 m/s depending on the actual α– and β-values.

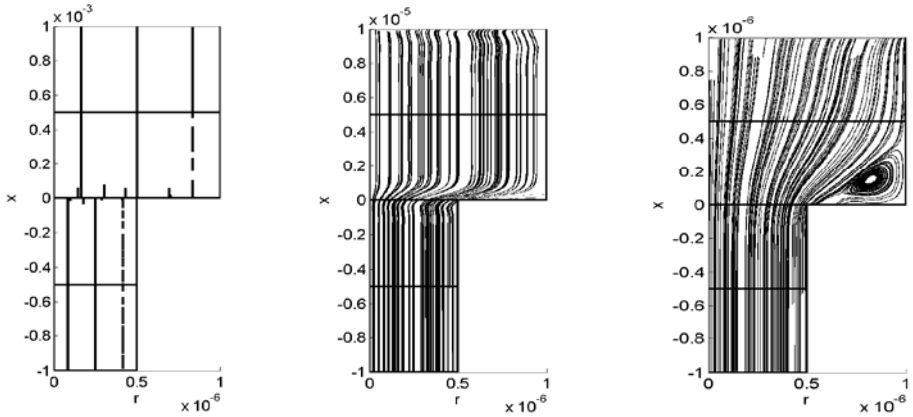

a) Model $E_{l=10^{-3}}$ b) Model $E_{l=10^{-5}}$ c) Model $E_{l=10^{-6}}$

Figure 6: NSE-Streamline velocity fields for modesl $E_{l=10^{-3},10^{-5},10^{-6}}$, (water flows upwards)

Figure 6 is quite representative of the general finding of the numerical simulations; little turbulence at the intersections unless the smallest tube length is very small (10^{-6}) and approaching the size of its radius. When the cross section of a pipe is relatively small, for example $r_1, r_2 = (1\times10^{-6}, 0.5\times10^{-6}\, m)$, the flow still is laminar with a sudden

contraction/expansion in cross sectional area, in spite of a large variation of the section length, $l_{1,2} = 10^{-3} \rightarrow 10^{-5} m$. Irregular fields are seen at a sudden change in section geometry as Figs.5(c) for $l_1 = l_2 \approx 10^{-6}$, that is when $\alpha_{1,2}$ increases or, as in our case, the section length is dramatically decreased with respect to the cross section area so that $l_i \approx r_i,\ i = 1,2$. The deviation of flow determined by the analytical model from the numerical solution could become in the order of 10 %. Furthermore, all velocities of the contraction models $C_{l=10^{-2}\rightarrow 10^{-6}}$ are faster than the corresponding expansion models $E_{l=10^{-2}\rightarrow 10^{-6}}$ That is, the suction at the front is more important than the flow resistance for these geometries. Based on these simulations with a variety of pipe intersection [6], it is clear that the analytical model (AE) is a very good model for the approximation of flow as the fluid passes section changes.

COMPARING CAPILLARY SUCTION EXPERIMENTS AND MODELING

Concrete data and laboratory measurements of water suction on dry concrete slices

Experiments with one sided capillary absorption were performed with two different concrete qualities. Specimens were produced from ordinary portland cement (ASTM Type II/CEM I 42,5 R) with blaine specific surface 384 m^2/kg, granitic aggregate with 8 mm maximum size, 9% fines less than $0.125mm$ and 0.5% absorption and a co-polymer water reducer (Sika Viscocrete) added to obtain flowable consistency. Two different mortar mixes were made with $w/c = 0.45$ and 0.60 respectively. Both mixes had 39 vol-% cement paste and 2 % air voids. Cylindrical specimens with diameter 100 mm and height 200 mm were cast in two layers in steel molds with slight compaction on a vibrating table between each layer. The cylinders were de-moulded after 24 hours and cured in water at 20^oC for approximately four months. Then, slices with thickness 20, 40 and 100mm where wet-sawn normal to the cylinder axis. The slices were dried at 105^oC to constant weight, air cooled to room temperature and quickly sealed on their lateral surfaces to ensure undirectional flow of water. For each material and thickness four specimens were weighed regularly. The capillary suction curves for slices of different thickness of the w/c = 0.60 are shown in Figure 1. The suction porosities of the specimens were measured after the capillary absorption tests by total immersion until constant weight. Volumes were determined by weighing in water. Then degree of hydration (*hyd* in eq.(25) [18]) was solved based on the Powers model [19]:

$$p_{tot} = (w/c - 0.172hyd)/(w/c + 1/\rho_c) \quad (25)$$

ρ_c is particle density of cement. Finally, the capillary porosities were determined according to Powers model with eq. (26) [18]:

$$p_{cap} = (w/c - 0.415\alpha)/(w/c + 1/\rho_c) \quad (26)$$

Table 1 shows the results indicating that capillary porosity makes up around 40 % of the total porosity for our specimens according to the differentiation between gelpores (where meniscii do not exist)- and capillaries based on Powers and Brownyard [19].

Table 1: Porosity (m^3/m^3) *and degree of hydration in the mortars*

w/c	p_{tot}	$p_{capillary}$	hyd
0.45	0.16	0.064	0.78
0.60	0.18	0.068	1.0

This means that in the order of 60% of the pore volume could be filled by other mechanism(s) than capillary suction. (Due to the water curing of the cylinders the factor 0.415 in eq.(26) should probably be reduced towards 0.357 which yields for filling of self-dessiccation pores. So the capillary porosities of table 4 are probably a bit low and the difference too small between w/c = 0.45 and 0.60.) The pipe suction model can only work in capillaries so the gel porosity is obviously a source of error. Nevertheless we believe that our model gives information about the possibility for pore necks to cause the capillary absorption anomaly (deviation from linear absorption-√time and vanishing nick points) since our specimens contained large fractions of capillaries.

Comparing measured capillary suction with calculations for different pipe geometries

In order to study the influence of the pipe geometry on the absorption of water, we constructed first several contraction-expansion sections (Model C) and expansion-contraction (Model E), see Figure 5. The resulting pipe-geometries are illustrated in Figure 7.

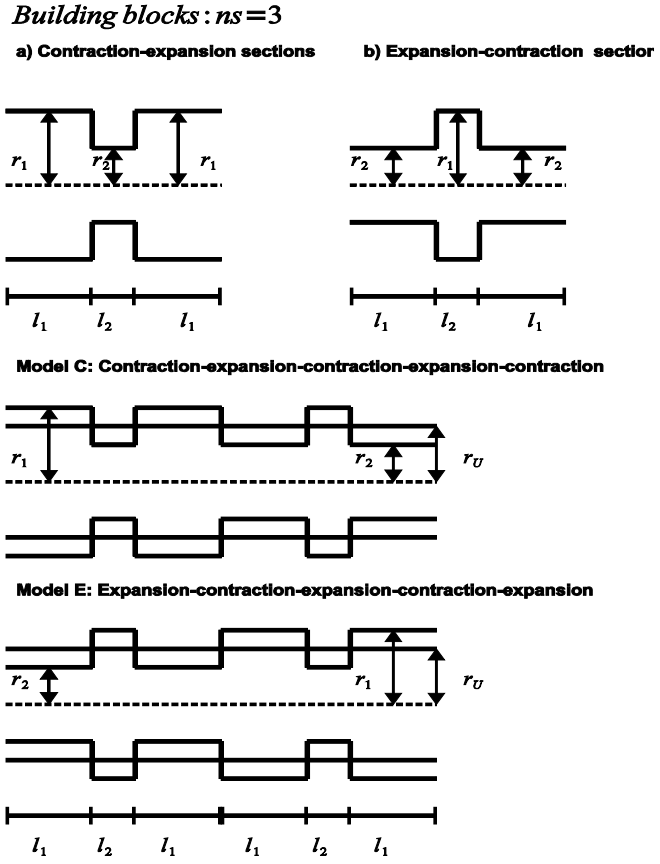

Figure 7- Model C, E with $ns = 3$, $N = 6$ *sections and Model U with constant radius*

As shown in Figure 7, two different combinations of sections (a) and (b) give the structure of models C-E. Each combination has $(ns - N)$ sections. Also a mean uniform radius giving the same pipe volume was constructed. When plotting the calculated absorption as (kg/m^2) vs square root time the absorption may simply be interpreted as a suction height to be compared with the results of eqs.(21) - (24). This is also a way to interpret experimental, one sided, absorption. To compare calculations with experiments where the pore volume varies depending on w/c, degree of hydration and fraction of cement paste (assuming non-porous

aggregate) we then simply calculate the absorption in the form of weight. The above mentioned mean pipe radius was calculated for each C- and E-models. This gives a mean porosity (this was also done for a random sized pore model, see [6,7]). Absorption measured in lab was always compared with calculated absorption in different pipe systems at equal total porosity by using mean pipe radii. For each set of models C or E, there is a corresponding model-U with the constant uniform mean volume radius r_U. We require the conservation of volume for these three models. Let V_C, V_E and V_U denote the volume for model C, model E and model U, respectively. In order to have the same volume for all three models, the radius r_U must satisfy the following condition:

$$V_C = V_E = V_U \Rightarrow \frac{1}{2}\pi(r_1^2 + r_2^2) = \pi\, r_U^2 \;\Rightarrow\; r_U = \sqrt{\frac{r_1^2 + r_2^2}{2}}. \tag{27}$$

We observe that the radius r_U depends only on the radii r_1 and r_2 but not on the section lengths l_1 and l_2 .The volume (V) of the capillary absorbed water is then calculated by eq.(28) with $\Delta h_j(t)$ defined by eq. (21):

$$V(t) = \sum_{i=1}^{j-1} \pi r_i^2 l_i + \pi r_j^2 \Delta h_j(t) \tag{28}$$

Before comparing the model with experiments, absorption was calculated in a wide range of analytical C- and E- models [6,7]. These results showed that the right kind of deviation from straight-line (absortion-√t) could be obtained for realistic pipe sizes, - lengths and time scales. Fig. 8 compares calculated capillary suction for two different pipe geometries with measured absorption in the $w/c = 0.60$ specimens .

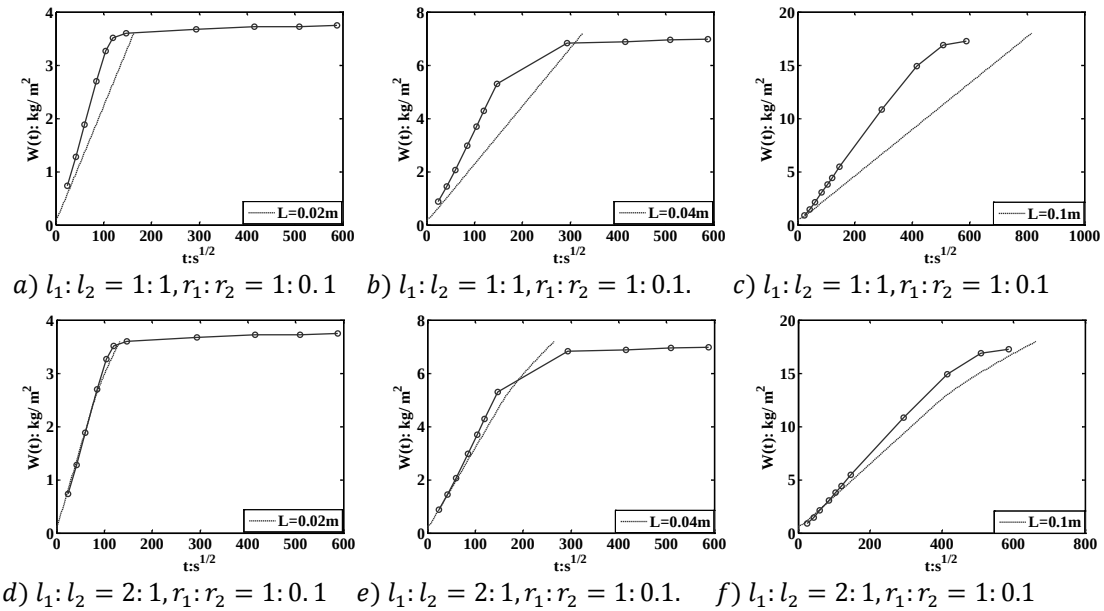

a) $l_1 : l_2 = 1:1, r_1 : r_2 = 1:0.1$ *b)* $l_1 : l_2 = 1:1, r_1 : r_2 = 1:0.1$. *c)* $l_1 : l_2 = 1:1, r_1 : r_2 = 1:0.1$

d) $l_1 : l_2 = 2:1, r_1 : r_2 = 1:0.1$ *e)* $l_1 : l_2 = 2:1, r_1 : r_2 = 1:0.1$. *f)* $l_1 : l_2 = 2:1, r_1 : r_2 = 1:0.1$

Figure 8- Analytical (dashed lines, Model C) and Experimental (full lines with circles) water absorption curves $(W(t) - \sqrt{t})$ *for* $w/c = 0.60$ *, and for three different pipe/specimens length/thickness, and* $p_{tol} = 0.18$*. Note different scales depending on specimen thickness L*

In Figure 8 the ratio of radii between large and small pipes is constant at $1:0.1$ or $1\times10^{-6}\,m : 0.1\times10^{-6}\,m$, whereas the main pipe geometry variation between the upper and lower 3 figures is the length ratios between large and small pipes. Figure 8 shows that the calculated absorption approaches the measured absorption as the length ratio between the

large and small pipes increases from 1:1 to 2:1. It is very interesting to note that the calculated capillary suction seems to give the right kind of increasing anomaly at increasing suction length, i.e at increasing specimen thickness. Apparently the increased number of necks has the right kind of effect compared to what is commonly seen in capillary suction experiments on concrete. Figure 9 below shows the same type of plots as in Figure 8 for $w/c = 0.45$.

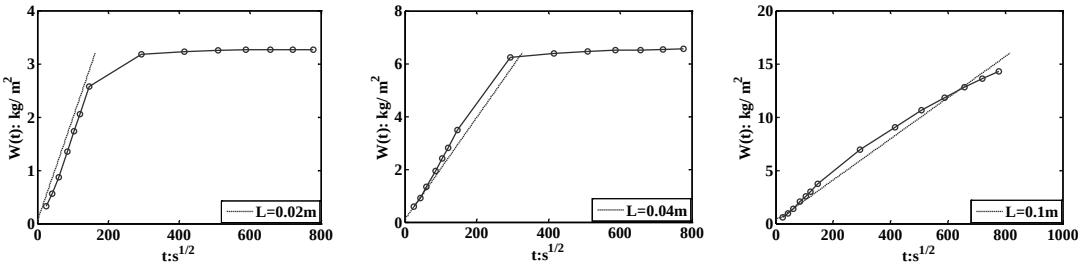

a) $l_1 : l_2 = 1:1, r_1 : r_2 = 1:0.1$ *b)* $l_1 : l_2 = 1:1, r_1 : r_2 = 1:0.1.$ *c)* $l_1 : l_2 = 1:1, r_1 : r_2 = 1:0.1$

Figure 9- Analytical (dashed lines, Model C) and Experimental (full lines with circles) water absorption curves $(W(t) - \sqrt{t})$ *for* $w/c = 0.45$*, 3 different pipe/specimen length/thickness, and* $p_{tot} = 0.16$., l_1:l_2=2:1,r_1:r_2=1:0.1, *Note different scales depending on specimen thickness L*

From Figure 9 we see that a slightly different pipe geometry with similar length of the large and small pipes fits the measured absorption best for w/c = 0.45. That is, compared to Figure 8 with w/c = 0.60, a somewhat larger fraction of smaller pores in $w/c = 0.45$ with less continuity is represented by this geometry. Figure 10 shows experimental capillary suction data from the literature [2,3] together with the model. The first concrete has $w/b = 0.40$ and 2 % condensed silica fume, and so has a low fraction, if any, of capillary porosity.

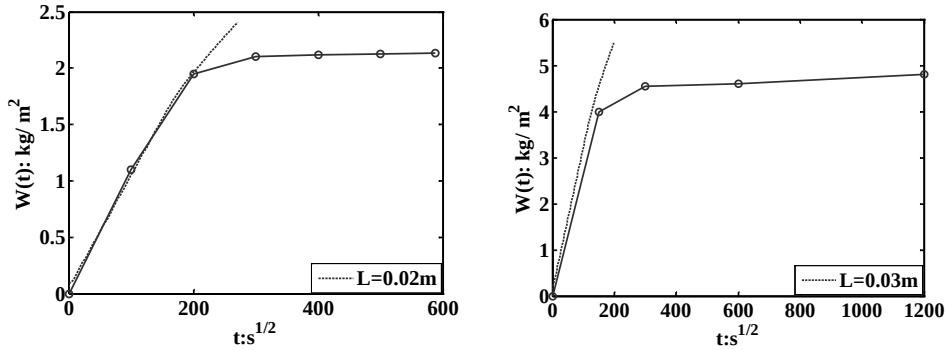

a)l_1:l_2=2:1,r_1:r_2=1:0.07 *[3]* *b)* $l_1 : l_2 = 2:1, r_1 : r_2 = 1:0.1$ *mortar [2]*

Figure 10 - Experiments [3,2] (full lines) and analytical (dashed lines) water absorption a) w/b = 0.40 and 2 % SF and $p_{tot} = 0.12$., *b) mortar w/c = 0.40 and* $p_{tot} = 0.18$.

From Figure 10 a) it can be seen that the changing of pipe geometry that worked successfully with high w/c in Figures 8 and 9 with 1:0.1 ratio between radii and a bit longer large pipe - sections is less successful and the small pipe has to be made even thinner. The reason could be the slow capillary suction in these specimens due to even more narrow necks than in $w/c = 0.45$. Figure 10 b) shows experimental capillary suction data of ordinary portland cement mortar with $w/b = 0.40$ taken from [2] showing a bit faster suction than the specimens with 2 % silica fume [3], pressumably due to higher cement paste volume fraction in the mortar as well as coarser OPC binder and more ITZ in the (OPC) mortar.

The total length of the model pipes compared to the thickness of the specimen is a matter of uncertainly. We have in our comparisons between calculated and experimental capillary suction used a total pipe length equal to the thickness of the specimens. Due to factors such as entrapment of air in a network and torturousity, it seems obvious that the straight C and E models are not right. Clearly more work in the calculation of the correct total absorption should be made. We believe, however, that the present investigation indicates that the kind of narrowing or pore-neck effect proposed can at least partly explain the deviation from the square root time law often seen in concrete capillary suction experiments.

Size limit of suction by water tensile strength, effective pore-size, multi-scale

There is a physical limitation to the use of capillary rise simply calculated from the suction p_c created in the pore water under the curved meniscus, eq. (4). This limitation is the minimum pore size of a water meniscus where the tensile strength of water $\sigma_{H_2 0}$ is exceeded so that the meniscus breaks down. The tensile strength of water has been measured: $\sigma_{H_2 0} \approx 0.5 N/mm^2$ at $20^o C$ [20]. Then solving eq.(4) with zero degree contact angle gives the minimum capillary pore radius r_{min} for a maximum suction equal to the tensile strength of water, eq.(29):

$$max\ p_c = \sigma_{H_2 o} = \frac{2\sigma_{l-g}}{r_{min}} \Rightarrow r_{min} = \frac{2\sigma_{l-g}}{\sigma_{h_2 o}} \quad \text{so} \quad r_{min} = \frac{2 \times 0.073 \frac{N}{m}}{0.5 \frac{N}{mm^2}} \approx 3 \times 10^{-4} mm \approx 0.3\ \mu m \tag{29}$$

We see that the minimum capillary radius with a meniscus creating suction calculated this way is similar to the minimum radius used in the above calculations. We therefore assume that capillary theory based on Laplaces law applies to our pipes.

The results also demonstrate a contradiction between the restriction of capillary theory due to the tensile strength of water (minimum capillary pore size approximately $3 \times 10^{-7} m$) and the application of a sort of "effective uniform capillary radius" or “effective pore-size” which is calculated as low as $10^{-11} m$ when applying eq.(22) to experimental data, see also [1,3,4,10,21,22]. This scale problem is possibly solved to a large part by the accumulated effect of repeated necks with high flow resistance, possibly together with some kind of slow diffusion mechanism filling the gel-type pores smaller than those filled by the capillary mechanism and slow filling of large air voids by some other mechanism. Gel filling could be further investigated with some sort of diffusion-loss from the water in the pipe-shaped pores into the pipe walls made of gel-material, whereas absorption into large air voids could be due to a different filling mechanism. Use of one or two additional transport (multi-scale) mechanisms could still keep the model on a relatively simple yet realistic and sound physical basis. However, an algorithm or calculation method requiring little computational power has to be developed so that a simultaneous gel-capillary-macro pore absorption model could calculate transport as fast as the present model.

CONCLUSIONS

Capillary suction was modeled with a relatively simple analytical pipe model consisting of series of pipes with different diameters and lengths put together in a regular manner. The objective was to investigate the slowing down of capillary absorption compared to linear (absorption- $\sqrt{t}$) plots. This occurs at increasing specimen thickness and reduced w/b and could be explained by repeated narrow pore necks.

First a multiple pipe flow model based on repeated series of pipes with varying radii and lengths was developed. Suction under water meniscii according to Laplace was used as driving force for flow. The flow calculated by this analytical pipe model was then compared with numerical simulations. The simulations allowed analysis of the effect of local flow conditions (development of flow profile, turbulence) and showed that the analytical model works satisfactorily. Then, a systematic comparison was made between calculated aborption for different model-pipe systems and real capillary absorption data from own experiments as well as some experimental data from the literature.

Realistic time scales for capillary filling can be obtained for series of pipes consisting of only large and small pipes of diameter in the order 1 and 0.1 microns, respectively. There has to be somewhat larger length than radius for the larger pipe in order to fit capillary suction for $w/c = 0.60$ compared to $w/c = 0.45$. The calculated capillary absorption then fits our experimentally measured absorption in slices with different thickness (20,40 and 100 mm), in line with the increased number of necks with increasing thickness and higher fraction of coarser capillary pores at heigh w/c. The results of some comparisons with experiments from the literature were in line with the comparisons with own experiments, including both the effect of silica fume (pore refinement) and ITZ (mortar with increased amount of capillaries).

The capillary suction size limitation by tensile strength of water was found to be acceptable for our models (minimum $r \approx 0.3$ microns). However, the effective averge size that can be calculated from observed concrete absorption rates ($r \approx 0.1$ Å) is far too small. Possibly this can be dealt with by adding another diffusion type transport mechanism in the gel into a extended, multi-scale, model. Also the very slow filling of large air voids should be included.

ACKNOWLEDGEMENT

This work is based on the PhD of the first author “Water and heat transfer in cement based materials” H.T. Nguyen, PhD Thesis University of Tromsø, 2011, ISBN 978-82-8236-030-02, ISSN 978-82-8236-031-9

REFERENCES

1. Hoff, W. D.; Hall, C.(2002): Water transport in brick, stone and concrete. *Spon press London and New York*, 318p.
2. Hazrathi , K. (1998): Etudes des mechanismes de transport de l'eau par absorption capillare dans des materiaux cimentaries conventionels et de haute performance, PhD, Laval University, Canada

3. Sellevold, E.J.; Punkki, J. (1994): Capillary suction in concrete: Effects of drying procedure, Nordic Concrete Research Publication (15) 59-74
4. Garboczi, E. Bentz, D. (1999): Computer simulation and percolation theory applied to concrete. Annual reviews of computational Physics VII, World Sc. Publ. comp. 85-123. www.nist.gov
5. Hansic, L. (2005): Capillarity in concrete, PhD, University of Lubljana.
6. Nguyen H.T., Melandsø F., Jacobsen S.(2010) Capillary suction in concrete with analytical pipe model – part 1: numerical study of flow conditions, Nordic Concrete Research Publication 42(2) 71-87
7. Nguyen H.T., Melandsø F., Jacobsen S.(2010) Capillary suction in concrete with analytical pipe model – part 2: Expansion-, contraction- and random sized sections compared with experiments, Nordic Concrete Research Publication 42(2) 89-107
8. Durst, F.; Loy, T. (1985): Investigation of laminar flow in a pipe with sudden contraction of cross sectional areal. Computers and Fluids (13) 15-36
9. Dullien, F. A. L.; El-Sayed, M. S.; Batra V. K. (1976): Rate of Capillary Rise in Porous Media with Nonuniform Pores. Journal of Colloid and Interface Science (60) 497-506
10. Fagerlund, G.(1991): Unpublished data cited by E.J. Sellevold in course compendium post graduate course Concrete Structure. Norwegian Univ. of Science and Technology, Dept of Concrete Structures
11. Frank, P. Incropera; David, P. DeWitt (2002) Fundamentals of Heat and Mass Transfer, Fifth Edition John Wiley and Sons. Inc.
12. Chatterje, S. (2002) An explanation for the unsaturated state of water stored concrete, Cement and Concrete Composites (26) 75-79
13. Merle, C. Potter, David, C. Wiggert (1991) Mechanics of Fluids, Prentice Hall
14. Wen-Bin Young. (2004) Analysis of capillary flows in non-uniform cross-sectional capillaries. Colloids and Surfaces A: Physicochem. Eng (234) 123-128
15. Karoglou, M., Moropoulou, A., Giakoumaki, A., Krokida, M.K. (2005) Capillary rise kinetics of some building materials. Colloids and Interface Science (284) 260—264
16. Barbare, Nikhil, Shukla, Aru,; Bose, Arijit (2003) Uptake and loss of water in a cenosphere-concrete composite material. Cem and Conc Res (33) 1681-1686
17. Comsol Multiphyscis 3.2 (2005) COMSOL AB
18. Sellevold E.J., Farstad T. (2005) The PF-method-A simple way to estimate the w/c-ratio and Air content of Hardened Concrete. Mindess Symposium ConMat Conference, UBC, Vancouver Canada
19. Powers, T. C.; Brownyard, T. L.(1948) Bulletin 22, Res. Lab. Portland Cem. Ass., Skokie, Illinois
20. Crum, L. A. (1979) Tensile strength of water, Nature (278) 148-149
21. Fagerlund, G. (1982) On the capillary of concrete, Nordic Concrete Research Journal (1) 20 p.
22. Martys N., Ferraris C.F (1997) Capillary transport in mortars and concrete, Cement and Concrete Research (27) 747-760